Moving Horizon Estimation for Integrated Navigation Filtering ⋆

Tomáš Polóni [*,**] **Boris Rohaľ-Ilkiv** [**] **Tor Arne Johansen** [***]

[*] *Department of Aerospace Engineering, University of Michigan, Ann Arbor, USA*
(e-mail: tpoloni@umich.edu)
[**] *Institute of Automation, Measurement and Applied Informatics; Faculty of Mechanical Engineering; Slovak University of Technology; Bratislava; Slovakia*
(e-mail:boris.rohal-ilkiv@stuba.sk)
[***] *Center for Autonomous Marine Operations and Systems (AMOS) Department of Engineering Cybernetics; Norwegian University of Science and Technology; Trondheim; Norway*
(e-mail: Tor.Arne.Johansen@itk.ntnu.no)

Abstract: This paper presents a nonlinear numerical observer for accurate position, velocity and attitude (PVA) estimation including the accelerometer bias and gyro bias estimation. The Moving Horizon Observer (MHO) processes the accelerometer, gyroscope and magnetometer measurements from the Inertial Measurement Unit (IMU) and the position and velocity measurements from the Global Navigation Satellite System (GNSS). The nonlinear measurement equations with the rotation matrix, expressed through the quaternion parametrization, in combination with the state-space rigid body kinematic model of translational and rotational motion is the subject of optimization defined on a receding data window. The gradient-based trust-region method is applied to solve the MHO's nonlinear least-squares criterion. The MHO is tesed off-line in the numerical experiment involving the experimental flight data from a light fixed-wing aircraft. This study demonstrates the quality of the MHO computations with the comparison of the reference filter, the multiplicative Extended Kalman Filter (EKF).

Keywords: State estimation, Attitude estimation, Position estimation, Moving horizon observer

1. INTRODUCTION

Integrating a Global Navigation Satellite System (GNSS) with an Inertial Navigation System (INS) is the state-of-the-art in the navigation systems and this topic has been studied intensively in the literature. The formulation of attitude estimation is known as the Wahba problem, defined as the batch vector-data estimation problem Wahba (1965). Commonly used algorithms, Crassidis et al. (2007) to solve for the attitude estimation problem (the Wahba problem) are QUEST-based algorithms Shuster and Oh (1981); Bar-Itzhack (1996); Psiaki (2000); Christian and Lightsey (2010), Extended Kalman filtering (EKF) algorithms Lefferts et al. (1982); Markley (2003); Markley and Sedlak (2008), Unscented Kalman filtering (UKF) algoritms Crassidis and Markley (2003), Rhudy et al. (2013) or more computationally advanced particle filters (PF) Cheng and Crassidis (2004), Carmi and Oshman (2009) based on the Bayesian theory. Recently also nonlinear observers are developed in Grip et al. (2013) and further discussed in references therein.

The moving horizon observer (MHO), Rao et al. (2003); Alessandri et al. (2008), is an interesting and potentially attractive alternative to the EKF and particle filter statistical methods, Cheng and Crassidis (2004); Carmi and Oshman (2009). Like the EKF method, MHOs are usually based on a least squares (minimum variance) cost function. While the EKF leads to recursive update equations for the estimate and its error covariance matrix based on the most recent measurement of output and inputs, the MHO differs in two important ways. First, it considers a finite moving window (horizon) of data when updating the estimates rather than just the most recent sample. Second, it directly minimizes the least squares cost function using nonlinear programming rather than deriving a recursive update formula based on linearization. MHO may be considered more powerful than EKF since it is less dependent on linearization, it may be able to capture non-white noise characteristics due to its moving window of measurements that will make correlations apparent, and due to its ability to directly incorporate constraints on the estimate, Haseltine and Rawlings (2005). In the meaning of MHO, batch estimation with trust-region algorithm has been proposed in Psiaki and Hinks (2012) where the idea of outer numerical solution for the angular velocity vector updates the inner analytical solution for the quaternion.

⋆ This work is supported by the Slovak Research and Development Agency under projects APVV-0090-10 and APVV-0015-12. This work is also supported by the Research Council of Norway through the Center of Excellence on Autonomous Marine Operations and Systems (AMOS), grant 223254, and project grant 221666.

The MHO has been recently studied for the attitude estimation in Vandersteen et al. (2013).

The main contribution of this paper is the formulation of a MHO for the position, velocity and attitude computation, combining the GNSS, magnetometer and IMU sensors and the experimental evaluation of such formulation, whereas Vandersteen et al. (2013) uses only the gyroscope and magnetometer information. The Global Positioning System (GPS) is used by the GNSS receiver, measuring the position and velocity, while the accelerometer, gyroscope and magnetometer represent the IMU measurements. The method is experimentally off-line tested on the aircraft data and compared with the performance of the multiplicative Extended Kalman Filter, Markley (2003). It is shown that the MHO converges faster than the multiplicative EKF from the incorrect initial conditions and that the MHO with a moderately precise MEMS IMU can perform equivalently to the multiplicative EKF using the gyroscope and accelerometer data set from a relatively more precise MEMS IMU, where both, the EKF and the MHO use the same GNSS measurements.

The Euclidean norm is denoted as $\|\cdot\|_2$. For a vector $x \in \mathrm{R}^3$, $S(x)$ denotes the skew-symmetric matrix

$$S(x) = \begin{bmatrix} 0 & -x_3 & x_2 \\ x_3 & 0 & -x_1 \\ -x_2 & x_1 & 0 \end{bmatrix}$$

A unit quaternion $q = [s_q r_q]^T$ is defined by a scalar part $s_q \in \mathrm{R}$ and a vector part $r_q \in \mathrm{R}^3$. A multiplication of the quaternions q and p is defined through the quaternion product

$$q \otimes p = \begin{bmatrix} s_q s_p - r_q^T r_p \\ s_q r_p + s_p r_q + r_q \times r_p \end{bmatrix}$$

For a vector $x \in \mathrm{R}^3$, $\tilde{x}$ denotes the quaternion with scalar part zero and vector part x, i. e., $\tilde{x} = [0, x]^T$. A vector $x \in \mathrm{R}^3$ decomposed in the coordinate system a is denoted x^a. The same vector decomposed in the coordinate system b is denoted x^b. The rotation between these coordinate systems is expressed through a unit quaternion $q_a^b = [s_{q_a^b} r_{q_a^b}]^T$. The rotation matrix $R(q_a^b) \in SO(3)$ is given as $R(q_a^b) = I + 2s_{q_a^b} S(r_{q_a^b}) + 2S(r_{q_a^b})^2$ such that $R(q_a^b)x^a = x^b$. The rate of rotation of the coordinate system marked with the subscript b with respect to the coordinate system a, decomposed in c, is symbolized by ω_{ab}^c. Four coordinate systems are going to be referred in this paper: Earth-Centered Inertial (ECI), Earth-Centered Earth-Fixed (ECEF), North-East-Down (NED), and Body-Fixed (BODY) coordinate systems, with corresponding indices i, e, n, and b.

2. BASIC MODEL FORMULATION

In the next section the MHO is formulated to estimate the PVA based on the kinematic equations of the body in motion, Bekir (2007) (pp. 75-85), and measurements.

The system equations for translational rigid body dynamics are given as

$$\dot{p}^e = v^e \tag{1}$$

$$\dot{v}^e = -2S(\omega_{ie}^e)v_e + a^e + g^e(p^e) \tag{2}$$

where p^e is the position in ECEF coordinates, v^e is the linear velocity in ECEF coordinates, a^e is linear acceleration in ECEF coordinates and g^e is the gravity vector in ECEF coordinates. The gravity vector is a function of the position and it is modeled using the J_2 gravity model, Hsu (1996). The known Earth's angular velocity around the ECEF z-axis is represented by vector ω_{ie}^e. The system equations for rotational rigid body dynamics are represented as

$$\dot{q}_b^e = \frac{1}{2} q_b^e \otimes \tilde{\omega}_{ib}^b - \frac{1}{2} \tilde{\omega}_{ie}^e \otimes q_b^e \tag{3}$$

The position and velocity are considered in the ECEF frame and the rotation vector, the unit quaternion, is representing the rotation from BODY to ECEF frame.

The measurement equations with measurement noise are

$$\omega_m^b = \omega^b + \alpha + \varepsilon_\omega \tag{4}$$

$$a_m^b = R(q_b^e)^T a^e + \beta + \varepsilon_a \tag{5}$$

$$m_m^b = R(q_b^e)^T m^e + \varepsilon_m \tag{6}$$

$$p_m^e = p^e + \varepsilon_p \tag{7}$$

$$v_m^e = v^e + \varepsilon_v \tag{8}$$

The biases are assumed to satisfy

$$\dot{\alpha} = 0 \tag{9}$$

$$\dot{\beta} = 0 \tag{10}$$

The position p^e, linear velocity v^e and magnetic field m^b are assumed to be measured without bias.

For the convenience of a more compact notation the state space model is written

$$\dot{x} = f_c(x, u) \tag{11}$$

where $f_c : \mathbb{R}^{n_x} \times \mathbb{R}^{n_u} \to \mathbb{R}^{n_x}$ represents the augmented dynamics Eq. (1)-(3) and Eq. (9)-(10), $x = [p^e, v^e, q_b^e, \alpha, \beta]^T$ is the state vector and $u = [a^e, \omega^b]^T$ is the input. The observation Eq. (4)-(8) may be written as

$$y = h_c(x, u) + \varepsilon \tag{12}$$

where $y \in \mathbb{R}^{n_y}$ is the vector of measurements $y = [\omega_m^b, a_m^b, m_m^b, p_m^e, v_m^e]$ and $h_c : \mathbb{R}^{n_x} \times \mathbb{R}^{n_u} \to \mathbb{R}^{n_y}$ is a continuous measurement function. The measurement errors are given in the vector $\varepsilon = [\varepsilon_\omega, \varepsilon_a, \varepsilon_m, \varepsilon_p, \varepsilon_v] \in \mathbb{R}^{n_y}$. The situation encountered in practice is when the system is governed by continuous-time dynamics and the measurements are obtained at discrete time instances. For the MHO formulation, the Euler method discretized nonlinear dynamic system is considered

$$p^e(i) = p^e(i-1) + \tau v^e(i-1) \tag{13}$$

$$v^e(i) = v^e(i-1) + \tau \left[a^e(i-1) + g^e - 2S(\omega_{ie}^e)v^e(i-1)\right] \tag{14}$$

$$\begin{aligned} q_b^e(i) = {} & q_b^e(i-1) \\ & + \frac{\tau q_b^e(i-1)}{2} \begin{bmatrix} 0 & -\omega_{ib}^{b,T} \\ \omega_{ib}^b & -S(\omega_{ib}^b) \end{bmatrix} \\ & - \frac{\tau q_b^e(i-1)}{2} \begin{bmatrix} 0 & -\omega_{ie}^{e,T} \\ \omega_{ie}^e & S(\omega_{ie}^e) \end{bmatrix} \end{aligned} \tag{15}$$

$$\alpha(i) = \alpha(i-1) \tag{16}$$

$$\beta(i) = \beta(i-1) \tag{17}$$

where i represents the numerical step index, and τ is the numerical step size. Eq. (13)-(17) can be written in the form

$$x(k+1) = f(x(k), u(k)) \tag{18}$$

$$y(k) = h(x(k), u(k)) + \varepsilon(k) \tag{19}$$

for discrete time index $k = 0, 1, \ldots$, where $x(k) \in \mathbb{R}^{n_x}$ is the augmented state vector and $u(k) \in \mathbb{R}^{n_u}$ is the input vector. The state vector is observed through the measurement equation (19) where $y(k) \in \mathbb{R}^{n_y}$ is the observation vector and $\varepsilon(k) \in \mathbb{R}^{n_y}$ is a measurement noise vector. For convenience, it is assumed that all sensors operate at the same rate, i. e. interpolated data are generated for the slower sensors. The common discretization interval (sampling period) is denoted T_s.

3. MOVING HORIZON OBSERVER

Assuming the quaternion parametrization of the rotation matrix $R(q_b^e)$, a least-squares criterion for the moving horizon observer is formulated at time index k as minimizing of J with respect to $\hat{p}^e(k-N), \hat{v}^e(k-N), \hat{q}_b^e(k-N), \{\hat{a}^e(t)\}_{t=k-N}^k, \{\hat{\omega}^b(t)\}_{t=k-N}^k, \hat{\alpha}(k-N), \hat{\beta}(k-N)$ where

$$\begin{aligned}
J = & \sum_{t=k-N}^{k} ||\omega_m^b(t) - \hat{\omega}^b(t) - \hat{\alpha}(t)||_{W_1}^2 \\
& + \sum_{t=k-N}^{k} ||R(\hat{q}_b^e(t))a_m^b(t) - \hat{a}^e(t) - R(\hat{q}_b^e(t))\hat{\beta}(t)||_{W_2}^2 \\
& + \sum_{t=k-N}^{k} ||R(\hat{q}_b^e(t))m_m^b(t) - m^e||_{W_3}^2 \\
& + \sum_{t=k-N}^{k} ||p_m^e(t) - \hat{p}^e(t)||_{W_4}^2 + \sum_{t=k-N}^{k} ||v_m^e(t) - \hat{v}^e(t)||_{W_5}^2 \\
& + ||1 - ||\hat{q}_b^e(k-N)||_2^2||_{W_6}^2 \\
& + ||\bar{\alpha}(k-N) - \hat{\alpha}(k-N)||_{W_7}^2 \\
& + ||\bar{\beta}(k-N) - \hat{\beta}(k-N)||_{W_8}^2 \\
& + ||\bar{a}^e(k-N) - \hat{a}^e(k-N)||_{W_9}^2 \\
& + ||\bar{\omega}^b(k-N) - \hat{\omega}^b(k-N)||_{W_{10}}^2 \\
& + ||\bar{p}^e(k-N) - \hat{p}^e(k-N)||_{W_{11}}^2 \\
& + ||\bar{v}^e(k-N) - \hat{v}^e(k-N)||_{W_{12}}^2 \\
& + ||\bar{q}_b^e(k-N) - \hat{q}_b^e(k-N)||_{W_{13}}^2
\end{aligned} \tag{20}$$

is computed using forward-Euler numerical integration of motion dynamics, Eq. (13)-(17), and the quaternion constraints

$$\begin{bmatrix} -1 \\ -1 \\ -1 \\ -1 \end{bmatrix} \leq \hat{q}_b^e \leq \begin{bmatrix} 1 \\ 1 \\ 1 \\ 1 \end{bmatrix} \tag{21}$$

The cost function comprises of two kinds of terms. The first kind of term is the one that considers the whole horizon; this is characterized by the sum in front of the norm. This kind of term is useful if new information from sensors should have a dominant effect on the estimates. The second kind of term is known as the regularizing cost and in general introduces the cost of change of the estimates at the beginning of moving horizon window in the time instance $k-N$, where N is the length of horizon. The regularizing term is useful for its filtration effect of the estimates. Each term has its weight W that represents the significance of each term value that builds the overall cost function value. The length of horizon represents the memory window of the measured data and it can be chosen depending on the sampling interval and dynamic response. The weights W should be chosen with respect to all signal errors magnitudes. The length of horizon N and values of weights W are recommended to be set via tuning and test procedures. In addition, square of quaternion elements add up to 1, meaning any unit quaternion satisfies $\|\hat{q}_b^e\|_2^2 = 1$, which is enforced by a penalty term.

The optimized variable is the state at the beginning of the horizon window $\hat{p}^e(k-N), \hat{v}^e(k-N), \hat{q}_b^e(k-N), \hat{\alpha}(k-N), \hat{\beta}(k-N)$ with the optimal model response, Eq. (13)-(17), referred to as the N-step model prediction. The estimated variables that enter the N-step model prediction as the unknown inputs are the acceleration $\{\hat{a}^e(t)\}_{t=k-N}^k$ and angular velocity vectors $\{\hat{\omega}^b(t)\}_{t=k-N}^k$. From the optimization point of view the acceleration and angular velocity vectors are estimated as the free variables.

The a priori state estimate used in the regularizing cost at the beginning of the horizon is declared as $\bar{x}(k-N) = [\bar{p}^e, \bar{v}^e, \bar{q}_b^e, \bar{\alpha}, \bar{\beta}]^T$ and is computed in a time instant k for the time instance $k-N$ by means of simulation as a one step prediction

$$\bar{x}(k-N) = f(\hat{x}(k-N-1), u(k-N-1)) \tag{22}$$

where

$$u(k-N-1) = \begin{bmatrix} R(\hat{q}_b^e(k-N-1))a_m^b(k-N-1) \\ \omega_m^b(k-N-1) \\ -R(\hat{q}_b^e(k-N-1))\hat{\beta}(k-N-1) \\ -\hat{\alpha}(k-N-1) \end{bmatrix} \tag{23}$$

and $\hat{x}(k-N-1)$ is the optimal estimate at the previous update. The a priori angular velocity estimate $\bar{\omega}^b(k-N)$ and a priori acceleration estimate $\bar{a}^e(k-N)$ used in the regularizing cost at the beginning of the horizon is set in a time instant k for the time instance $k-N$ from the previous optimal estimates of ω^b, a^e (estimated in time instance $k-1$) as

$$\bar{a}^e(k-N) = \hat{a}^e(k-N-1) \tag{24}$$

$$\bar{\omega}^b(k-N) = \hat{\omega}^b(k-N-1) \tag{25}$$

Consequently, the variables for the time instant $k-N-1$ are not the subject of optimization in the time instance k.

A gradient-based trust-region-reflective method Nocedal and Wright (2006) (pp. 76-77), is applied to solve the nonlinear-least square MHO criterion, Eq. (20). The gradients are computed numerically by finite differences within the iterative process to solve for the scaled modified Newton step that arises from examining the Kuhn-Tucker necessary conditions defined for the box constraint problem, see the `lsqnonlin` function Matlab (2012). The number of iterations in an optimization depends on a solver's stopping criteria. The stopping criteria for this method is a relative tolerance δ_J on the cost function value $J(x)$ where the iterations stop if $|J(x_i) - J(x_{i+1})| < \delta_J(1 + |J(x_i)|)$. The other stopping parameter of the optimization metric is δ_x, which is a relative bound on the size of a step, meaning that iterations end when $|x_i - x_{i+1}| < \delta_x(1 + |x_i|)$. The parameters that contribute significantly to the precision of the trust-region-reflective method are maximum δ_{max} and minimum δ_{min} perturbation in variables for

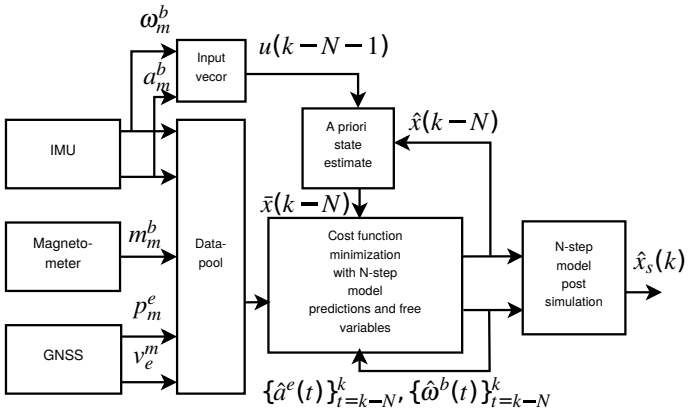

Fig. 1. Algorithm scheme of MHO

finite-difference gradients computations. Finite-differences used to estimate gradients are computed with the central method. The number of fixed iterations and the number of function evaluations of the trust-region-reflective method is implicitly limited through the above mentioned parameters. The specified maximum allowed number of iterations Λ can be considered as one of the tuning parameters for the amount of filtering.

The MHO algorithm scheme is shown in Figure 1. The algorithm can be summarized into following steps:

(1) `Initialization`; $k = N + 1$;
- Load the initial Datapool with measurement data
- Set the initial values $\hat{x}(0) = [\hat{p}^e(0), \hat{v}^e(0), \hat{q}_b^e(0), \hat{\alpha}(0), \hat{\beta}(0)]^T$ for the a priori state estimate, Eq. (22) (more details are discussed in section 4.2)
- Compute the initial input vectors $\hat{a}^e(0)$ and $\hat{\omega}^b(0)$ according to Eq. (23)

(2) `Start main loop`; Increment $k \leftarrow k + 1$;
- Obtain the output measurement $y(k)$ and update the Datapool
- Numerically integrate a priori state estimates $\bar{x}(k-N)$ with Eq. (22)-(23)
- Set the a priori inputs $\bar{a}^e(k-N)$ and $\bar{\omega}^b(k-N)$ from the previous iteration, Eq. (24), (25)

(3) `Optimization`.
- Set the initial guess for the iterative nonlinear optimization $\hat{x}^{init}(k-N) = \bar{x}(k-N)$.
- Minimize the cost function (20) to numerically compute the optimal state vector estimate $\hat{x}(k-N)$ and at the very beginning of the receding window and to estimate the input vectors $\{\hat{a}^e(t)\}_{t=k-N}^k, \{\hat{\omega}^b(t)\}_{t=k-N}^k$ on the whole horizon. When computing the cost function, the model is used for prediction through the Eq. (13)-(17), similar to a direct single shooting strategy.

(4) `Post-simulation to obtain` $\hat{x}_s(k)$.
- The initial condition for the first step is $\hat{x}_s(k-N) = \hat{x}(k-N)$.
- Use the model to estimate the state from the beginning of the window $k-N$ to the end of the window k as

$$\hat{x}_s(k-N+i) = f\left(\hat{x}_s(k-N+(i-1)), u(k-N+(i-1))\right) \quad (26)$$

where $i = 1, 2, \ldots, N$ and

$$u(k-N+(i-1)) = \begin{bmatrix} \hat{a}^e(k-N+(i-1)) \\ \hat{\omega}^b(k-N+(i-1)) \end{bmatrix} \quad (27)$$

(5) `End of loop`; Go to Step 2.

Conditions for convergence and stability of the Moving Horizon Observer (MHO) are established in the literature for the case when open loop prediction models are applied Sui and Johansen (2011); Alessandri et al. (2008); Rao et al. (2003) as in this case, Eq. (13)-(17). Like the EKF, the key conditions are uniform observability (i.e. observability of the system, and persistent excitation of the data) as well are optimality of the solution found of the numerical optimization problem. The latter requires that the initialization of the a priori estimate is sufficiently accurate, and generally means that only local convergence can be established. This is not a computationally most efficient implementation, but serves the purpose of comparing performance indicators such as convergence speed and accuracy.

To be able to use or display the outputs of the MHO to a user or to a control system it is sometimes convenient to express the estimates of the PVA in the NED coordinates. With respect to the WGS-84 reference ellipsoid, the position estimate $\hat{p}^e$ is transformed into the estimates of latitude $\hat{\mu}$, longitude $\hat{l}$ and height $\hat{h}$. This transformation is computed via an iterative procedure, such as that of Hofmann-Wellenhof, Lichtenegger, and Collins, Hofmann-Wellenhof et al. (2001) (pp. 279-303), where only one iteration at each sampling interval is performed. The relation between the ECEF and NED coordinate rotation is given as

$$\hat{q}_e^n(k) = \hat{q}_\mu(k) \otimes \hat{q}_l(k) \quad (28)$$

where $\hat{q}_\mu = [\cos((\hat{\mu} + \pi/2)/2); 0; \sin((\hat{\mu} + \pi/2)/2); 0]$ and $\hat{q}_l = [\cos(\hat{l}/2); 0; 0; -\sin(\hat{l}/2)]$. Following, the velocity in the NED coordinate system is computed as

$$\hat{v}^n(k) = R(\hat{q}_e^n(k))\hat{v}^e(k) \quad (29)$$

as well as the attitude expressed in the NED coordinate system is given as

$$\hat{q}_b^n(k) = \hat{q}_e^n(k) \otimes \hat{q}_b^e(k) \quad (30)$$

4. EXPERIMENTS

The presented MHO algorithm is experimentally tested on the flight data from the aircraft. The experiments are performed on the Piper Cherokee 140 light fixed-wing aircraft, Grip et al. (2013).

4.1 Setup and Implementation

The aircraft is carrying the Xsens MTi inertial measurement unit mounted on a bulk head in the back, and the uBlox LEA-6H GNSS receiver with an active antenna mounted on the instrument panel. The Xsens MTi is equipped with a moderately accurate accelerometer, gyroscope and magnetometer with an in-run gyro bias stability of 20 deg.h^{-1}. The position as well as Doppler-based velocity measurement is provided by the uBlox LEA-6H GNSS receiver. The Xsens MTi measurements are provided at the sampling interval 0.01 s and the uBlox LEA-6H GNSS module provides the measurements at the

sampling interval 0.2 s. All the sensor readings are filtered using thirdorder low-pass filters with a cutoff frequency of 5 Hz, and the GPS readings are resampled to 0.01 s before being provided to the observer. The magnetometer measurements are also filtered with a fourth-order notch filter to remove the predominant component of a square disturbance with period 1.2 s, caused by the aircraft's anti-collision light.

The benchmark algorithm considered in this study is the multiplicative EKF that provides a reference for the MHO estimates. The EKF processes measurements from a set of higher-quality sensor ADIS 16488 "tactical grade" IMU. The position and Doppler-based velocity measurement is provided by the uBlox LEA-6H GNSS receiver. The ADIS sensor is mounted within the cockpit behind the pilot's seat. The ADIS 16488 contains relatively accurate accelerometers, gyros, and magnetometers, with an in-run gyro bias stability of 6.25 deg.h^{-1}. The measurements are obtained at the sampling rate of 410 Hz and downsampled to 100 Hz. Magnetometer readings are provided by the Xsens MTi instead of the ADIS 16488, due to the difficulty of accurately calibrating magnetometers installed in the cockpit. The EKF is implemented as an indirect filter with resetting, but with both prediction and update taking place at 100 Hz. The EKF estimates PVA, gyro bias and accelerometer bias. The attitude is represented by a quaternion in the navigation equations, whereas the attitude error in the EKF is represented using a 3-DOF Gibbs vector. The attitude quaternion is reset in the style of a multiplicative EKF, Markley (2003).

The experimental flight data lasts approx. 40 min.

4.2 Settings and Results

The MHO is evaluated and tested in comparison with the multiplicative EKF in the following experiments. One main challenge for each observer/filter is how fast will the states (and other optimized variables) converge, therefore the initialization of the MHO plays an important role. As already mentioned, the initial state vector estimate $\hat{x}(0)$ (this vector should not be confused with the initial value for the optimization $\hat{x}^{init}$) can be set from the sensors. The initial position and velocity are set from the GPS measurement while the initial quaternion vector is indirectly set from the accelerometer and magnetometer unit vectors and their references $a^e_{ref} = [3.058; 5.971; -7.130]$ m.s^{-2} and $m^e_{ref} = 10^4[2.644; 4.085; -2.468]$ nT based on the QUEST algorithm described in Shuster and Oh (1981). The initial inputs $\hat{a}^e(0)$ and $\hat{\omega}^b(0)$ are always set according to the Eq. (23).

Experiment 1 The first experiment considers the run of the MHO that starts its computations 15 min after the take off and the computations run 23.3 min. The initial conditions, set from the sensors, are set sufficiently close to the reference values given by the EKF. The EKF runs its computations from the very first sample instant, starting during the airplane's take off and having ample time to converge. The comparison of attitude estimation of the MHO and the reference EKF is shown in Figure 2. The settings for MHO are shown in Table 1.

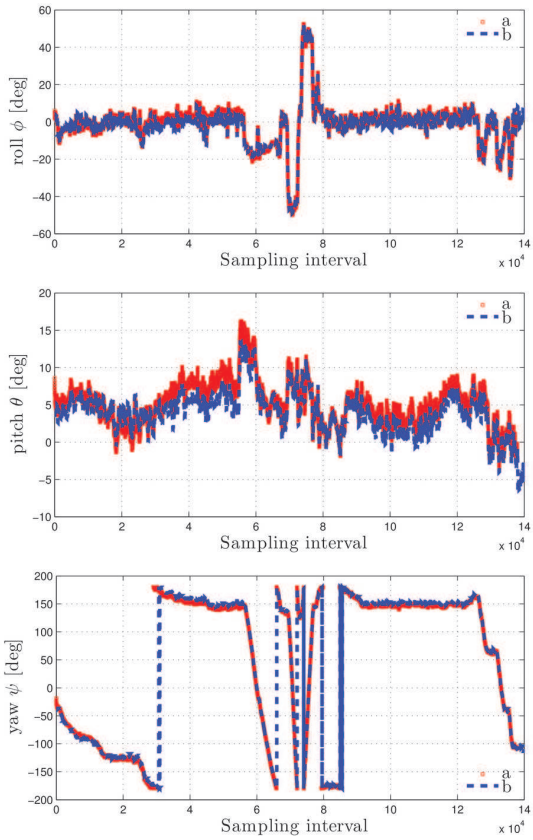

Fig. 2. Estimated Euler angles, a - MHO, b - EKF (reference)

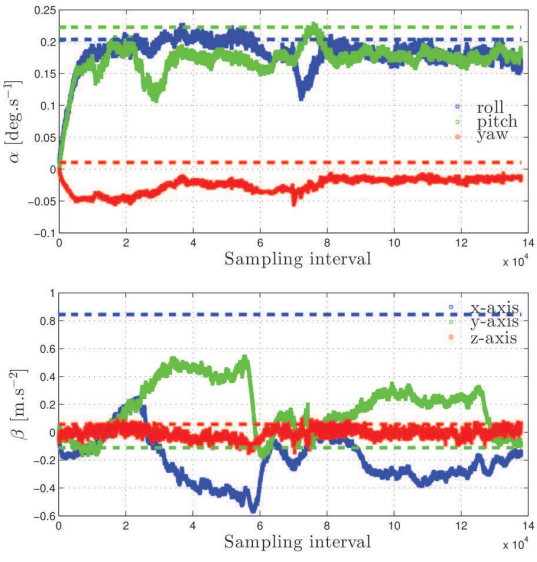

Fig. 3. Estimated biases by MHO. The reference values were obtained as the mean values from the airplane's stand still gyroscope and accelerometer recordings right after the landing and are displayed as dashed lines. These reference values have informative character.

Parameter	Setting	Description
τ	0.01	Integration step
Λ	16	Maximum number of iterations
N	3	Length of horizon
W_1	$5 * 10^3 I_3$	Gyroscope weight
W_2	$20 * 10^3 I_3$	Accelerometer weight
W_3	$5 * 10^3 I_3$	Magnetometer weight
W_4	$2I_3$	Position weight
W_5	$2I_3$	Velocity weight
W_6	0.1	Quaternion weight
W_7	$10^4 I_3$	Gyroscope bias weight
W_8	$10^1 I_3$	Accelerometer bias weight
W_9	$5 * 0.01 I_3$	Acceleration regularizing cost
W_{10}	$5 * 0.001 I_3$	Gyro regularizing cost
W_{11}	10^2 if $J < \delta_T$	Position regularizing cost
W_{12}	10^2 if $J < \delta_T$	Velocity regularizing cost
W_{13}	10^2 if $J < \delta_T$	Quaternion regularizing cost

Table 1. Setting of main tuning parameters for MHO

Estimated sensor biases are displayed in Figure 3. The tuning of the MHO's parameters is important for the overall performance of the observer. Tuning of the MHO in Table 1 overestimates the pitch angle θ shown in Figure 2 in comparison with the reference EKF. This can be explained by more relaxed tuning of the accelerometer bias weight W_8 and conservative tuning of the acceleration regularizing cost W_9. The pitch angle θ, in Figure 2 is overestimated at the same time intervals as the accelerometer bias in y-axis, in Figure 3, deviates from the reference. The accelerometer bias is not observable in all conditions and requires moves with sufficient excitations in the given axis. If the new weights W_8 and W_9 are set according to the tuning shown in Table 2, similar attitude estimation as the reference EKF is achieved. The attitude estimation is documented in Figure 4 with bias estimates documented in Figure 5. The regularization terms were not found in general to influence stability properties of the estimator.

Parameter	Setting	Description
τ	0.01	Integration step
Λ	16	Maximum number of iterations
N	3	Length of horizon
W_1	$5 * 10^3 I_3$	Gyroscope weight
W_2	$20 * 10^3 I_3$	Accelerometer weight
W_3	$5 * 10^3 I_3$	Magnetometer weight
W_4	$2I_3$	Position weight
W_5	$2I_3$	Velocity weight
W_6	0.1	Quaternion weight
W_7	$10^4 I_3$	Gyroscope bias weight
W_8	$10^2 I_3$	Accelerometer bias weight
W_9	$5 * 0.001 I_3$	Acceleration regularizing cost
W_{10}	$5 * 0.001 I_3$	Gyro regularizing cost
W_{11}	10^2 if $J < \delta_T$	Position regularizing cost
W_{12}	10^2 if $J < \delta_T$	Velocity regularizing cost
W_{13}	10^2 if $J < \delta_T$	Quaternion regularizing cost

Table 2. Setting of main tuning parameters for MHO

Experiment 2 The second experiment focuses on the convergence ability of the MHO, where the comparison with the benchmark reference EKF is continued. In this scenario, the initialization of the MHO after 29 min after take off is considered where the scenario lasts 8.3 min. The initial conditions, set from the sensors, are set

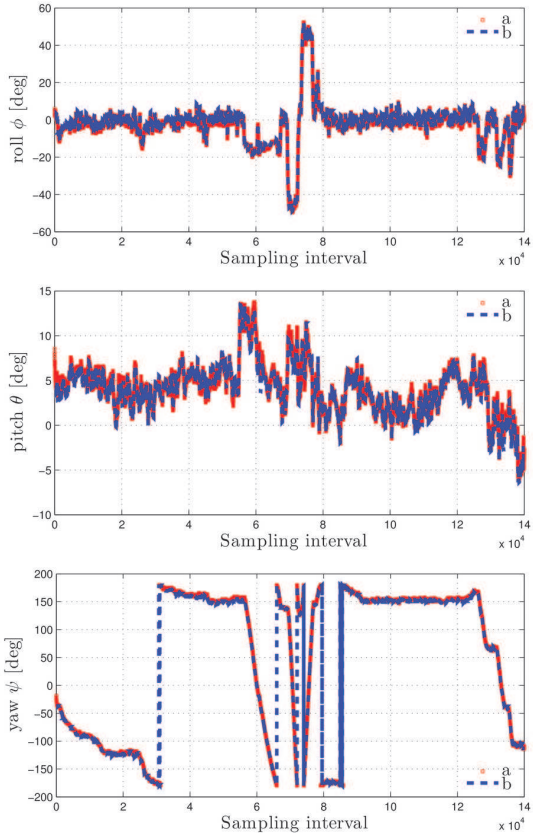

Fig. 4. Estimated Euler angles, a - MHO, b - reference EKF

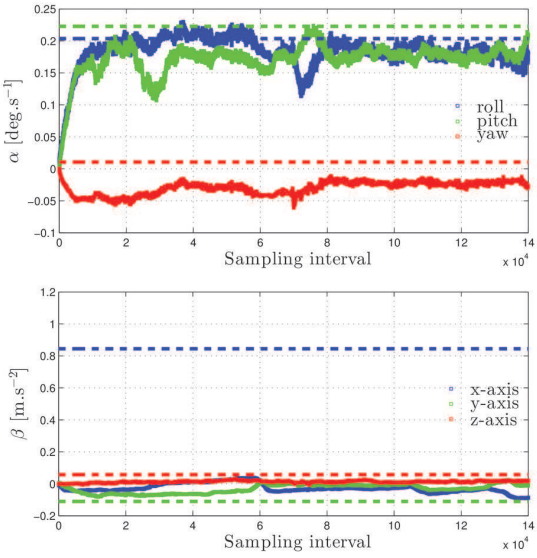

Fig. 5. Estimated biases

wrong due to noisy measurements of the accelerometer and magnetometer in comparison to the reference values given by the EKF. The reference EKF runs its computations from the very first sample instant, starting during the airplane's take off and having ample time to converge. The settings used by the MHO are presented in Table 2.

Beside the reference multiplicative EKF (d) and the MHO (b), the performance of the multiplicative EKF (a) and

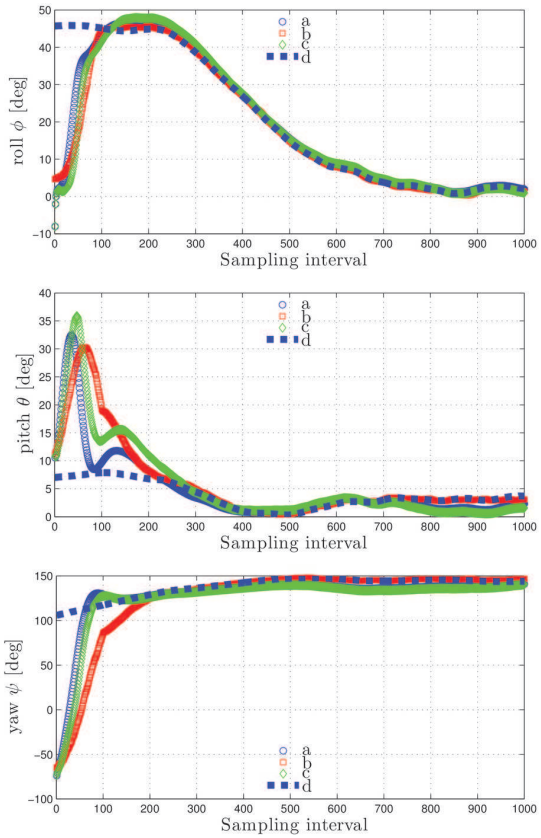

Fig. 6. Zoom of estimated Euler angles, a - EKF, b - MHO, c - EKF (with Xsens MTi), d - reference EKF

RSE of	roll $\phi \times 10^3$	pitch $\theta \times 10^3$	yaw $\psi \times 10^3$
a	0.2619	0.1591	0.9029
b	0.2970	0.1853	1.2274
c	0.3748	0.2183	1.1907

Table 3. Root Square Error for transient data in Fig. 6, first 250 sec, a-EKF (Adis 16488), b-MHO (Xsens MTi), c-EKF (Xsens MTi)

the multiplicative EKF with moderately accurate Xsens MTi IMU sensor set (c) is compared. The multiplicative EKFs (a,c) are initialized in the same sampling interval as the MHO (b) but the reference multiplicative EKF (d). Zoomed plots of the first 10 s are shown in Figure 6.

The performance in this experiment is evaluated by the Root-Square-Error index computed for each Euler angle as

$$RSE = \sqrt{\sum_{k=1}^{n} e_j^2(k)} \tag{31}$$

where $j = 1, 2, 3$, $n = 25000$, $e_1(k) = \phi_r(k) - \hat{\phi}(k)$ and $e_2(k) = \theta_r(k) - \hat{\theta}(k)$, $e_3(k) = \psi_r(k) - \hat{\psi}(k)$. The RSE index numbers for the first 250 s are shown in Table 3. The MHO (b) has shown a better performance in comparison to the multiplicative EKF (c) in terms of the roll ϕ and pitch θ angles and slightly worse performance in the yaw angle ψ. The MHO (b) and the multiplicative EKF (c) are both using the same IMU, Xsens MTi. The best performance for the first 250 s is delivered by the multiplicative EKF (a) using relatively precise IMU, Adis 16488.

RSE of	roll ϕ	pitch θ	yaw ψ
a	8.8331	28.1161	159.1960
b	80.9853	65.4003	249.4891
c	179.1406	66.3386	557.7118

Table 4. Root Square Error for steady-state data, last 250 s, a-EKF (Adis 16488), b-MHO (Xsens MTi), c-EKF (Xsens MTi)

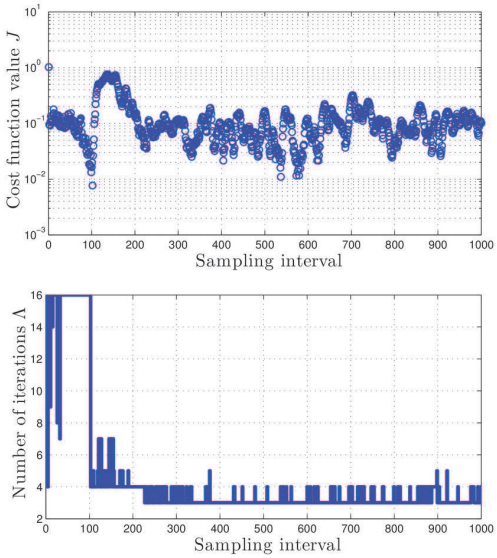

Fig. 7. Computational indicators

The RSE index numbers for the last 250 s are shown in Table 4. The MHO (b) has shown a better performance in comparison to the multiplicative EKF (c) in terms of all the Euler angles. The best performance for the last 250 s is delivered by the multiplicative EKF (a) using relatively precise IMU, Adis 16488.

The maximum number of iterations Λ is a tuning parameter needed for real-time computations when fixed-processing time is given by sampling intervals. Limiting the iterations thus leads to some trade-off between the speed of convergence and the speed of computations. In this case the regularization also reduces the number of iterations needed to attain optimality. The number of iterations with monitored cost function value for the first 10 s is plotted in Figure 7. These computational indicators are associated with zoomed plot shown in Figure 6. In order to improve the convergence of the MHO, the initial regularizing cost weights W_{11}, W_{12} and W_{13} are set to a very small number close to zero until the cost function reaches the threshold limit value δ_T. The cost function value is monitored during the computations and when it gets below the threshold value δ_T, the algorithm turns on the filtering by changing the regularizing cost weights W_{11}, W_{12} and W_{13}. It can be seen in Figure 6 that the convergence of the MHO (b) progresses fast until approx. 100th sampling interval when the cost function reaches the threshold value. This is when the regularizing cost weights are switched to their nominal values given in Table 2.

5. CONCLUSION

This work presents a novel methodology for estimation of position, velocity and attitude of a body in motion using

a moving horizon observer (MHO). The importance of MHO algorithm in combination with the motion dynamic equations and low-cost IMU and GNSS sensors lies in the simplicity of the problem formulation and in modularity of different sensor combinations for highly accurate estimation. The result of this study is a design and numerical off-line testing of the MHO on experimentally measured data as well as the favorable comparison with the reference multiplicative extended Kalman filter. The computational complexity and higher computational cost represents a key limitation when it comes to real-time estimations on such devices as CPU, GPU or FPGA. Higher computational costs are however inevitable in order to achieve better performance.

ACKNOWLEDGMENTS

The authors would like to thank to Håvard Fjær Grip, Jet Propulsion Laboratory, California Institute of Technology, for providing the data and consulting the implementation and measurement details.

REFERENCES

Alessandri, A., Baglietto, M., and Battistelli, G. (2008). Moving-horizon state estimation for nonlinear discrete-time systems: New stability results and approximation schemes. *Automatica*, 44(7). doi:10.1016/j.automatica.2007.11.020.

Bar-Itzhack, I.Y. (1996). REQUEST - a recursive QUEST algorithm for sequential attitude determination. *Journal of Guidance, Control, and Dynamics*, 19(5), 1034–1038. doi:10.2514/3.21742.

Bekir, E. (2007). *Introduction to Modern Navigation Systems*. World Scientific Publishing.

Carmi, A. and Oshman, Y. (2009). Adaptive particle filtering for spacecraft attitude estimation from vector observations. *Journal of Guidance, Control, and Dynamics*, 32(1), 232–241. doi:10.2514/1.35878.

Cheng, Y. and Crassidis, J. (2004). chapter Particle Filtering for Sequential Spacecraft Attitude Estimation. Guidance, Navigation, and Control and Co-located Conferences. American Institute of Aeronautics and Astronautics. doi:10.2514/6.2004-5337.

Christian, J.A. and Lightsey, E.G. (2010). Sequential optimal attitude recursion filter. *Journal of Guidance, Control, and Dynamics*, 33(6), 1787–1800. doi:10.2514/1.49561.

Crassidis, J.L. and Markley, F.L. (2003). Unscented filtering for spacecraft attitude estimation. *Journal of Guidance, Control, and Dynamics*, 26(4), 536–542. doi:10.2514/2.5102.

Crassidis, J.L., Markley, F.L., and Cheng, Y. (2007). Survey of nonlinear attitude estimation methods. *Journal of Guidance, Control, and Dynamics*, 30(1), 12–28. doi:10.2514/1.22452.

Grip, H., Fossen, T., Johansen, T., and Saberi, A. (2013). Nonlinear observer for GNSS-aided inertial navigation with quaternion-based attitude estimation. In *American Control Conference (ACC), 2013*, 272–279.

Haseltine, E.L. and Rawlings, J.B. (2005). Critical evaluation of extended Kalman filtering and moving-horizon estimation. *Ind. Eng. Chem. Res.*, 44(8), 2451–2460. doi:10.1021/ie034308l.

Hofmann-Wellenhof, B., Lichtenegger, H., and Collins, J. (2001). *Global Positioning System: Theory and practice*. Springer, 5th edition.

Hsu, D. (1996). Comparison of four gravity models. In *Position Location and Navigation Symposium, 1996., IEEE 1996*, 631–635. doi:10.1109/PLANS.1996.509138.

Lefferts, E.J., Markley, F.L., and Shuster, M.D. (1982). Kalman filtering for spacecraft attitude estimation. *Journal of Guidance, Control, and Dynamics*, 5(5), 417–429. doi:10.2514/3.56190.

Markley, F.L. (2003). Attitude error representations for Kalman filtering. *Journal of Guidance, Control, and Dynamics*, 26(2), 311–317. doi:10.2514/2.5048.

Markley, F.L. and Sedlak, J.E. (2008). Kalman filter for spinning spacecraft attitude estimation. *Journal of Guidance, Control, and Dynamics*, 31(6), 1750–1760. doi:10.2514/1.35221.

Matlab (2012). *Optimization Toolbox Release 2012b*. The MathWorks, Inc., Natick, Massachusetts, United States.

Nocedal, J. and Wright, S.J. (2006). *Numerical Optimization*. Springer, 2 edition.

Psiaki, M.L. (2000). Attitude-determination filtering via extended quaternion estimation. *Journal of Guidance, Control, and Dynamics*, 23(2), 206–214. doi:10.2514/2.4540.

Psiaki, M.L. and Hinks, J.C. (2012). Numerical solution of a generalized Wahba problem for a spinning spacecraft. *Journal of Guidance, Control, and Dynamics*, 35(3), 764–773. doi:10.2514/1.56151.

Rao, C.V., Rawlings, J.B., and Mayne, D.Q. (2003). Constrained state estimation for nonlinear discrete-time systems: Stability and moving horizon approximations. *IEEE Transactions on Automatic Control*, 48(2), 246–258. doi:10.1109/TAC.2002.808470.

Rhudy, M., Gu, Y., Gross, J., Gururajan, S., and Napolitano, M.R. (2013). Sensitivity analysis of extended and unscented Kalman filters for attitude estimation. *Journal of Aerospace Information Systems*, 10(3), 131–143. doi:10.2514/1.54899.

Shuster, M.D. and Oh, S.D. (1981). Three-axis attitude determination from vector observations. *Journal of Guidance, Control, and Dynamics*, 4(1), 70–77. doi:10.2514/3.19717.

Sui, D. and Johansen, T.A. (2011). Moving horizon observer with regularisation for detectable systems without persistence of excitation. *International Journal of Control*, 84(6), 1041–1054. doi:10.1080/00207179.2011.589081.

Vandersteen, J., Diehl, M., Aerts, C., and Swevers, J. (2013). Spacecraft attitude estimation and sensor calibration using moving horizon estimation. *Journal of Guidance, Control, and Dynamics*, 36(3), 734–742. doi:10.2514/1.58805.

Wahba, G. (1965). A least squares estimate of satellite attitude. *SIAM Review*, 7(3), 409–409. doi:10.1137/1007077.